

Detection of $H\alpha$ emission from $z > 3.5$ submillimetre luminous galaxies with *AKARI-FUHYU* spectroscopy

Chris Sedgwick¹, Stephen Serjeant¹, Chris Pearson^{2,1}, Ian Smail³, Myungshin Im⁴, Shinki Oyabu⁶, Toshinobu Takagi⁵, Hideo Matsuhara⁵, Takehiko Wada⁵, Hyung Mok Lee⁴, Woong-Seob Jeong⁷ and Glenn J. White^{1,2}

¹*Department of Physical Sciences, The Open University, Milton Keynes MK7 6AA, UK*

²*RAL Space, Rutherford Appleton Laboratory, Chilton, Didcot, Oxfordshire OX11 0QX, UK*

³*Institute for Computational Cosmology, Durham University, Durham DH1 3LE, UK*

⁴*Department of Physics and Astronomy, Seoul National University, Seoul 151-742, Korea*

⁵*Institute of Space and Astronautical Science, Japan Aerospace Exploration Agency, Sagami-hara, Kanagawa, 229 8510, Japan*

⁶*Graduate School of Science, Nagoya University, Furo-cho, Chikusa-ku, Nagoya, Aichi 464-8602, Japan*

⁷*Korea Astronomy & Space Science Institute, 776 Daedeok-daero, Yuseong-gu, Daejeon 305-348, Korea*

Re-submitted June 2013

ABSTRACT

We present tentative $H\alpha$ emission line detections of four submillimetre-detected galaxies at $z > 3.5$: the radio galaxies 8C1909+722 and 4C60.07 at signal-to-noise ratios (SNRs) of 3.1 and 2.5, and two submillimetre-selected galaxies (SMGs) near the first of these at SNRs of 10.0 and 2.4, made with the *AKARI Space Telescope* as part of the FUHYU mission program. These are the highest-redshift $H\alpha$ detections in such galaxies, made possible by *AKARI*'s unique near-infrared spectroscopic capability. The two radio galaxies had known redshifts and surrounding structure, and we have detected broad $H\alpha$ components indicating the presence of dust-shrouded quasars. We conclude that powerful AGNs at $z > 3.5$ occur in peaks of the star-formation density fields, supporting a close connection between stellar mass build-up and black hole mass assembly at this redshift. We also show that 4C60.07 is a binary AGN. The $H\alpha$ detections of the two SMGs are the first redshift determinations for these sources, confirming their physical association around their companion radio galaxy. The $H\alpha$ -derived star formation rates (SFRs) for the SMGs are lower than their far-infrared derived SFRs by a factor of ~ 10 , suggesting a level of dust obscuration similar to that found in studies at $\sim 1 < z < 2.7$.

Key words: galaxies: evolution — galaxies: starburst — galaxies: active — infrared: galaxies — submillimeter: galaxies

1 INTRODUCTION

The interaction between active galactic nuclei (AGNs) and star formation in galaxies is a key question in cosmology. For local galaxies, Magorrian et al. (1998) found a relation between black hole mass and stellar bulge mass, and Ferrarese & Merritt (2000) and Gebhardt et al. (2000) found a tight correlation between black hole mass and stellar velocity dispersion, so it is widely accepted that the two are intimately related. The redshift evolution of the cosmic star formation rate (SFR) is remarkably similar to that of quasar luminosity density (Boyle & Terlevich 1998; Chapman et al. 2005) and black hole accretion (Franceschini et al. 1999). Mid-infrared spectroscopy has shown that most Ultra-Luminous InfraRed Galaxies (ULIRGs, $10^{12} L_{\odot} < L_{IR} < 10^{13} L_{\odot}$) have simul-

taneous AGN and starburst activity in their nuclei (Genzel et al. 1998; Spoon et al. 2007).

Various models have been developed to explain the dynamics underlying these observations. Simulations of galaxy mergers have incorporated the growth of black holes and star formation, showing AGN feedback as a mechanism to regulate SFR (e.g. Springel et al. 2005; di Matteo et al. 2005). Semi-analytic source count models can best reproduce massive galaxy number densities when incorporating AGN feedback in the co-evolution of galaxies and their central black holes (e.g. Croton et al. 2006; Bower et al. 2006).

Observational constraints for such models from high-redshift galaxies are now becoming available. Studies using a combination of submillimetre and X-ray observations at $z \sim 2$ have confirmed the association of AGNs and intense star formation (Alexander et al. 2005; Harrison et al. 2012).

Table 1. Sample of high-redshift radio galaxies and submillimetre-selected sources. The 850 μm flux data from SCUBA and the target coordinates are from Stevens et al. (2003).

Source	RA (J2000)	Dec (J2000)	Redshift (z)	850 μm Flux (mJy)	— AKARI NIR Spectroscopy —		
					Observation ID	Dates	Exposure (mins)
8C1909+722 HzRG	19 08 23.3	+72 20 10.4	3.536 \pm 0.0003	34.9 \pm 3.0	1370153	8/2008(1), 8/2009(9)	93
SMMJ190827+721928 (SMM1)	19 08 27.4	+72 19 28.0	...	23.0 \pm 2.5	1370154	8/2008(10)	93
SMMJ190829+722050 (SMM2)	19 08 29.3	+72 20 49.6	...	8.7 \pm 2.4	1370155	8/2009(10)	93
SMMJ190816+722024 (SMM3)	19 08 16.1	+72 20 24.0	...	4.3 \pm 2.1	1370156	8/2008(5), 2/2009(2), 8/2009(3), 2/2010(3)	120
4C60.07 HzRG	05 12 54.8	+60 30 51.7	3.788 \pm 0.004	23.8 \pm 3.5	1370162	6/2008(9), 6/2009(1)	93

The discovery of high-redshift submillimetre galaxies (Smail et al. 1997; Hughes et al. 1998; Barger et al. 1998) and their possible association with high-redshift radio galaxies (HzRGs) (e.g. Stevens et al. 2003) implies that there are regions of intense star-formation which also show strong radio emission at high redshift. Detection of emission lines from these galaxies in the infrared can be used to confirm this connection, and to provide an independent measure of SFRs and AGN activity.

Spectroscopy of high-redshift radio and submillimetre galaxies has previously been made in the near-infrared K-band (Swinbank et al. 2004). The *AKARI Space Telescope* (Murakami et al. 2007) could obtain spectra at longer near-infrared wavelengths between 2.5 μm and 5.0 μm , a region not previously available for spectroscopy by other infrared space missions such as *Spitzer Space Telescope* (and with poor sensitivity from the ground), giving the possibility of detecting H α for galaxies at $3.0 < z < 6.5$.

This paper presents tentative H α detections from *AKARI* observations of high-redshift radio and submillimetre galaxies. Data collection and reduction are discussed in §2. Results are presented in §3 and discussed in §4. We assume $H_0=72.0 \text{ km s}^{-1}\text{Mpc}^{-1}$, $\Omega_M=0.3$ and $\Omega_\Lambda=0.7$.

2 DATA COLLECTION AND REDUCTION

2.1 AKARI-FUHYU Mission Program

The *AKARI* “Follow-Up Hayai-Yasui-Umai” mission program (FUHYU, Pearson et al. 2010) used the *AKARI* InfraRed Camera (IRC, Onaka et al. 2007) to carry out imaging and spectroscopy of well-studied galaxies rich in multi-wavelength data, often with known redshifts, to maximise the legacy value of the *AKARI* data. The mission program carried out extensive infrared imaging during the first two phases of the *AKARI* mission; the near-infrared spectroscopic campaign was carried out during Phase III, the warm phase after cryogen exhaustion. Spectroscopy was carried out using the IRC grism over a $1' \times 1'$ point source aperture centred on 46 submillimetre and radio galaxies from June 2008 - May 2010. We will be reporting later on results for the rest of our FUHYU mission program targets.

2.2 Targets Observed

Observations were made of two HzRGs, and three submillimetre sources potentially associated with one of them (see

Table 1 and Figure 1). Stevens et al. (2003) described submillimetre mapping of these radio sources by the Submillimeter Common-User Bolometer Array (SCUBA) instrument on the James Clerk Maxwell Telescope (JCMT), and suggested that the submillimetre sources observed were associated with the nearby radio source on the basis of their number densities and positions relative to the radio jets.

8C1909+722 and companions. The redshift was reported in De Breuck et al. (2001) based on a deep Keck optical spectrum showing strong Ly- α emission with FWHM = $1200 \pm 90 \text{ km s}^{-1}$. This field was included in an 850 μm survey of the environments of HzRGs which detected three nearby submillimetre galaxies (Stevens et al. 2003). Two of the three submillimetre sources (SMM1 and SMM2) were later detected at 350 μm with SHARC-II on the Caltech Submillimeter Observatory (Greve et al. 2006). A recent study using JVLA and IRAM PdBI radio observations and Herschel data at 100 μm - 500 μm (Ivison et al. 2012) found a large red dust feature aligned with the radio jet and SMM1, and concluded that SMM1 probably shared the same node or filament of the cosmic web as the radio galaxy, although it did not detect convincing ^{12}CO emission from SMM1. Redshifts for these SMGs were not previously known.

4C60.07. The redshift for this galaxy is based on the Ly- α emission line (Roettgering et al. 1997) with FWHM = $2880 \pm 940 \text{ km s}^{-1}$. Dust emission was detected at 850 μm and 1.25 mm (Papadopoulos et al. 2000), and CO J=1-0 emission (Greve et al. 2004). A detailed SMA, *Spitzer* and VLA study by Ivison et al. (2008) suggested an early-stage merger between the host galaxy of an AGN (the HzRG) and a companion starburst/AGN (which they labelled ‘B’; see Figure 3). They proposed that a second submillimetre source, which they labelled ‘A’, although of roughly equal integrated flux as source ‘B’, might be comprised of cold dust and gas, a short-lived tidal structure caused by the merger.

2.3 Observations

The *AKARI* IRC-NIR instrument used a filter wheel to select either one of three imaging filters or one of two dispersion elements. For our reference image, we used the *N3* image filter ($\sim 3 \mu\text{m}$) which had a field of view of approximately $10' \times 10'$ across 412×512 pixels giving a pixel scale of $1.46''$. For spectroscopy, we used the grism *NG* which dispersed between 2.5 μm - 5.0 μm across 291 pixels, giving $0.0097 \mu\text{m}$ per pixel, in a $1' \times 1'$ aperture (referred to as *Np*) which is

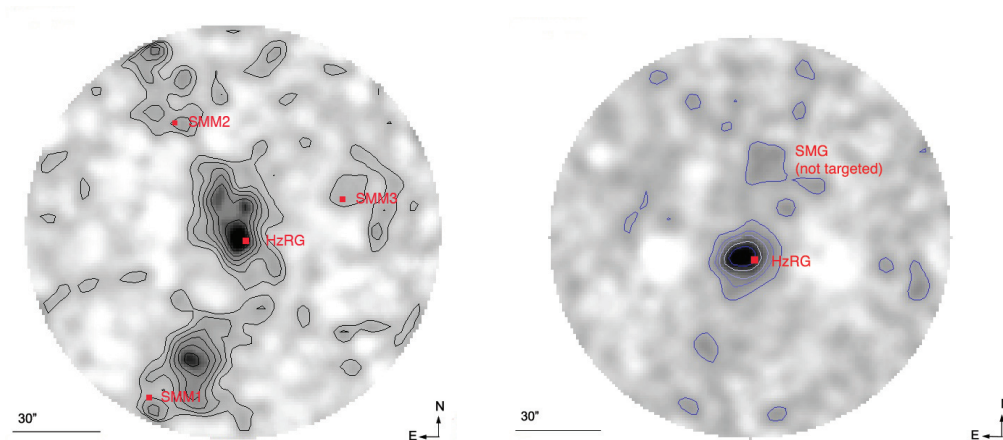


Figure 1. Left: SCUBA 850 μm image and contours (at 0.5, 1, 1.5, 2, 2.5 and 3 σ) for 8C1909+722 with the positions of the four AKARI spectra marked in red. Right: SCUBA 850 μm image and contours (at 1, 2, 3 and 4 σ) for 4C 60.07 with the position of the AKARI spectrum marked in red. This does not resolve the sources within the central contour (see Figure 3 for SMA 870 μm contours). The SCUBA maps are from Stevens et al. (2003).

dedicated to spectroscopy of point sources. The PSF FWHM was 4.7'' in imaging mode and $\sim 6.7''$ in spectroscopic mode.

We selected the spectroscopy Astronomical Observing Template (AOT) *IRCZ4* in the configuration *b;Np* (which selects the grism and the point source aperture). In Phase III, this configuration gives a 5 σ detection limit for point sources of ~ 2 mJy and a line sensitivity of $\sim 5 \times 10^{-18}$ Wm $^{-2}$ for each pointing. Each pointing consisted of a reference image (see Figures 2 and 3) and at least 8 exposure frames for the *NG* grism, bracketed by 10 dark frames (see Onaka et al. 2009 for details). Each frame exposure was ~ 70 seconds, giving an integrated exposure time for each pointing of ~ 9.3 minutes. We carried out 10 pointings per source wherever possible.

At the redshifts of the targets considered in this paper, the $H\alpha$ hydrogen recombination line falls within our 2.5 μm - 5.0 μm observed wavelength range. However, $H\beta$ was outside our range. No other emission lines were detected. We used the reference image of the larger 10' \times 10' N3 band field which is attached to the 1' \times 1' grism field, smoothed with a 5 \times 5 median boxcar, to confirm the identification of our sources with images from public archives.

2.4 Data reduction pipeline

The IRC data reduction pipeline for the warm phase (Onaka et al. 2009) was originally used to analyse our data. However, we found the correction for spacecraft jitter between the ~ 8 spectroscopic frames within each pointing and sky subtraction did not yield satisfactory results, so we wrote our own pipeline using Interactive Data Language (IDL) to reduce the raw spectroscopic data.

Our new pipeline includes dark subtraction, saturation masking (physical detector saturation is detected by scaled values from a short exposure and masked out), wavelength calibration and spectral response calibration using the calibration data from the IRC pipeline. We wrote our own routines to handle sky subtraction in which we fitted a sixth-order polynomial in the dispersion direction to remove a

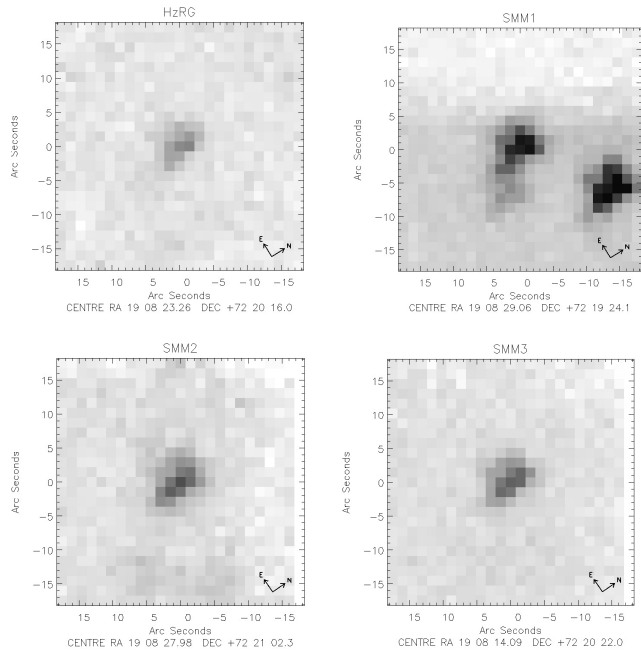


Figure 2. AKARI 3 μm images of the 8C1909+722 radio galaxy and its companion submillimetre galaxies. The figures are centred on the positional centroids of the spectra, and each is a median stack of the pointings taken for each source using the N3 filter. The dispersion direction is horizontal and the FWHM of the kernel used in the source extraction is equivalent to a width of 2 and 3 pixels in the wavelength and spatial directions respectively.

banding pattern across the frame, and a second-order polynomial in the image direction. We also wrote routines to handle de-glitching and to estimate the offsets between frames for each pointing caused by spacecraft jitter, using the simultaneous 10' \times 10' imaging data. Our pipeline included IDL routines for zerofootprint drizzling into a grid expanded by 5 times in each direction and for noise-weighted feature extraction which were previously developed for the SCUBA Half Degree Extragalactic Survey (SHADES, Serjeant et al.

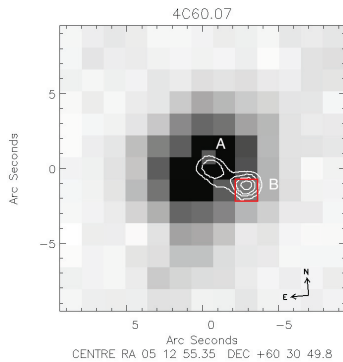


Figure 3. A blow-up of the *AKARI* 3 μm image of 4C60.07, overlaid by contours (at 3.5, 4.5, 5.5 and 6.5 σ) from the SMA 870 μm image for the centre of 4C60.07 from Ivison et al. (2008) which resolve the two submillimetre sources close to the HzRG. The labelling of the submillimetre sources ‘A’ and ‘B’ follows Ivison et al. (2008). The radio source overlaps ‘A’ and is centred $< 0.5''$ north-east of it. A red square marks the positional centre of the *AKARI* spectrum. The dispersion direction is horizontal and the FWHM of the kernel used in the source extraction was equivalent to a width of 2 and 3 pixels in the wavelength and spatial directions respectively.

2008), using a gaussian with a FWHM kernel in the expanded grid of 10 and 15 pixels in the wavelength and spatial directions respectively. This equates to a FWHM kernel of 2 and 3 pixels in the original data. We also wrote an IDL graphic user interface (GUI) routine to visualize various elements of the reduction on an interactive basis. Finally, the results were stacked by coadding the noise-weighted pointings for each target. The reduced spectra had lower noise and fewer artefacts than those from the *AKARI* pipeline.

The spectroscopic flat fields provided in the calibration data have low signal-to-noise and were found to increase the rms of our data slightly, so they were not used, following guidance in the manual (Onaka et al. 2009).

3 RESULTS

We show in Figure 4 the spectra of the five targeted sources, four of which appear to have significant $\text{H}\alpha$ emission. The spectra have been stacked by co-adding the noise-weighted pointings for each source. These spectra had been smoothed in the source extraction routine during the data reduction described in §2.4, and were not otherwise smoothed. The signal-to-noise ratios (SNRs) of these detections are 3.1 and 2.5 for the HzRGs and 10.0 and 2.4 for the submillimetre galaxies (see Table 2). Although some of the SNRs are relatively modest, the redshifts for the two HzRGs were already known from $\text{Ly-}\alpha$ and other emission lines (see §2.2) and all four $\text{H}\alpha$ line identifications were observed at the wavelengths corresponding closely to these redshifts. The estimated noise as a function of wavelength was calculated by splitting the raw data for each source into two halves and subtracting the two spectra obtained.

3.1 Spectra of the HzRGs

The spectrum for the radio galaxy 8C1909+722 HzRG has a broad $\text{H}\alpha$ emission line at the correct wavelength for its redshift, as shown in Figure 4 (top). The spectrum was taken from the centre of the target.

For the radio galaxy 4C60.07, Figure 3 shows the *AKARI* 3 μm image overplotted with the SMA 870 μm contours from Ivison et al. (2008). There are two submillimetre peaks, the weakest (labelled ‘A’) coincident with the 3 μm peak, and the strongest (‘B’) offset by about $3''$. The stacked spectrum for this radio source has a broad $\text{H}\alpha$ emission line at ‘B’ (see Figure 4, bottom). We did not detect an $\text{H}\alpha$ line at ‘A’.

The FWHM of the $\text{H}\alpha$ lines for the two HzRGs are shown in Table 2 and are $9400 \pm 1600 \text{ km s}^{-1}$ and $4800 \pm 1000 \text{ km s}^{-1}$ respectively, levels which show that dust-shrouded quasars are present in these sources.

3.2 Spectra of the submillimetre galaxies near 8C1909+722

SMM1 shows considerable structure, both in the submillimetre (see Figure 1) and at 3 μm (see Figure 2). The second-brightest of the submillimetre peaks shows an $\text{H}\alpha$ emission line, but the other peaks do not. The emission line confirms that SMM1 is at the same redshift as the radio galaxy.

SMM2 also shows $\text{H}\alpha$ emission (see Figure 4), again at the same redshift ($z = 3.536$), confirming that this galaxy is also associated with the radio galaxy. The spectrum for SMM2 is taken from the centre of the target in the *AKARI* 3 μm image.

SMM3 does not show a peak at the expected wavelength, although there is a strong peak about $0.05 \mu\text{m}$ lower. We have not taken this as a convincing $\text{H}\alpha$ emission line. Unlike SMM1 and SMM2, this galaxy is not aligned with the radio jets.

Stevens et al. (2003) suggested that the radio galaxy, the nearby submillimetre galaxies and other clumps had formed as a single galaxy cluster; we have confirmed that this association is correct in the case of two of these submillimetre sources.

3.3 Star Formation Rates

We have used the $\text{H}\alpha$ emission lines to estimate the star formation rates of the submillimetre galaxies, using the formula from Kennicutt (1998):

$$\text{SFR}/(M_{\odot}\text{yr}^{-1}) = 7.9 \times 10^{-35} L_{\text{H}\alpha}/W \quad (1)$$

assuming a Salpeter IMF and solar abundances. The results for the two submillimetre galaxies for which we detected $\text{H}\alpha$ lines are $260 \pm 80 M_{\odot} \text{ yr}^{-1}$ and $300 \pm 100 M_{\odot} \text{ yr}^{-1}$ respectively (see Table 2). No adjustment has been made for dust extinction.

We can obtain an alternative measure of the SFRs by using the 850 μm luminosity (Table 1) to estimate the 60 μm luminosity, then using the 60 μm luminosity to obtain an estimate of the far-infrared luminosity for 8-1000 μm (L_{FIR}). We have assumed the SED of the submillimetre galaxy SMMJ2135-0102 (the ‘Eyelash’) for these estimates,

Table 2. Estimates of star formation rates and line widths. Estimates of SFR($H\alpha$) for the SMGs are based on $H\alpha$ emission luminosities, and deconvolved FWHM are based on the width of the $H\alpha$ lines for the HzRGs. No adjustment for extinction has been made. FIR luminosities and SFRs are based on the 850 μm flux (see Table 1) assuming an SMMJ2135-0102 SED. SFR($H\alpha$)s for the HzRGs are not quoted due to line contamination from their AGNs. Redshifts in italics were identified by this work.

Source	Redshift (<i>z</i>)	Flux($H\alpha$) (10^{-19}Wm^{-2})	SNR($H\alpha$)	$L_{H\alpha}$ (10^{36}W)	SFR $_{H\alpha}$ ($\text{M}_{\odot}\text{yr}^{-1}$)	L_{FIR} ($10^{13}L_{\odot}$)	SFR $_{\text{FIR}}$ ($\text{M}_{\odot}\text{yr}^{-1}$)	FWHM($H\alpha$) (km s^{-1})
<i>HzRGs</i>								
8C1909+722 HzRG	3.536	7.9	3.1	8.6 ± 2.8	...	2.5 ± 0.2	4300 ± 1500	9400 ± 1600
4C60.07 HzRG	3.788	2.8	2.5	3.6 ± 1.4	...	1.7 ± 0.3	2900 ± 1000	4800 ± 1000
<i>SMGs</i>								
8C1909+722 SMM1	<i>3.536</i>	3.1	10.0	3.3 ± 0.3	260 ± 80	1.6 ± 0.2	2800 ± 1000	...
8C1909+722 SMM2	<i>3.536</i>	3.5	2.4	3.8 ± 1.6	300 ± 100	0.6 ± 0.2	1100 ± 500	...
8C1909+722 SMM3	...	<0.02	...	< 0.02	...	0.3 ± 0.2	500 ± 300	...

and then used the formula for estimating the star formation rate from Kennicutt (1998):

$$\text{SFR}/(\text{M}_{\odot}\text{yr}^{-1}) = 4.5 \times 10^{-37} L_{\text{FIR}}/W \quad (2)$$

The results of this calculation are shown in Table 2.

The SFRs estimated from $H\alpha$ are lower than the SFRs estimated from L_{FIR} by factors of about 11 and 4 respectively, suggesting dust obscuration. Swinbank et al. (2004) found an SFR(FIR)/SFR($H\alpha$) ratio of ~ 10 in a study of submillimetre to radio galaxies in the redshift range to $z = 1.408$ to $z = 2.692$. Takata et al. (2006) found close agreement between the two methods of estimating SFRs after adjusting the $H\alpha$ -based estimates for dust extinction by an average factor of 2.9 ± 0.5 in a study of submillimetre-selected ULIRGs at $0.9 < z < 2.7$. Figure 5 shows that our SMGs have luminosities and dust extinction at comparable levels with these earlier studies.

The total FIR luminosity calculated above also shows that SMM1 and the two HzRGs are HyperLuminous InfraRed Galaxies ($L_{\text{FIR}} > 10^{13}L_{\odot}$), and SMM2 is a ULIRG.

4 DISCUSSION AND CONCLUSIONS

These are the first (tentative) detections of $H\alpha$ emission lines in HzRGs / SMGs at $z > 2.8$.

We have found that the $H\alpha$ lines in the two HzRGs are broad. Broad $H\alpha$ emission lines in HzRGs are not rare (Larkin et al. 2000; Nesvadba et al. 2011) and indicate that these sources should be classified as reddened quasars rather than galaxies (see the discussion in Rawlings et al. 1995), a situation that can lead to misleading estimates of stellar populations in the host galaxy. This is a particular problem in studies using near-/mid-infrared photometry of sources which may otherwise appear to be narrow-line AGNs.

For 4C60.07, our detection of a broad $H\alpha$ line was at the location of the submillimetre source ‘B’ (see Figure 3). Ivison et al. (2008) suggested that ‘B’ was a gas-rich starburst/AGN on the basis of the red mid-infrared colours. Our discovery that ‘B’ is a quasar supports the argument that binary AGNs at close separations may be due to the triggering or enhancement of AGN activity during mergers. The unexpectedly high prevalence of binary quasars at high redshifts (Djorgovski 1991; Hennawi et al. 2010) provided strong support for this idea. A recent study of binary quasars found that simple halo occupation distribution

models under-predict quasar clustering at small separations (Kayo & Oguri 2012). That such a well-studied source had not previously been shown to be a quasar adds to the evidence that there is a higher fraction of binary AGN/quasars at high redshift than previously realised.

Our $H\alpha$ luminosity and FWHM results for the two HzRGs are both consistent with those of lower redshift radio galaxies (e.g. Nesvadba et al. 2011).

Our detection of $H\alpha$ emission lines from two submillimetre galaxies in the region of 8C1909+722 provides confirmation of their association with the HzRG. The extent of the system is ~ 700 kpc (based on Stevens et al. 2003), suggesting that this may be evolving into a cluster of galaxies or possibly a single galaxy. The complex SMM1 is ~ 80 kpc in extent and appears to be in the process of merging. In the 8C1909 field we have the first confirmation of multiple U/HyLIRGs in a protocluster region at $z > 3$, giving a combined SFR of $\sim 8000 \text{ M}_{\odot}\text{yr}^{-1}$.

The high levels of star formation in the two SMGs are shown with previous results in Figure 5. Our $H\alpha$ luminosities and SFR(FIR)/SFR($H\alpha$) ratios are comparable to those found in recent studies at $0.9 < z < 2.7$ suggesting similar levels of dust obscuration.

ACKNOWLEDGMENTS

This research is based on observations with *AKARI*, a JAXA project with participation of ESA. This work was supported by STFC under grant ST/G002533/1. IRS acknowledges support from STFC and the Leverhulme Trust. MI acknowledges support from the Creative Research Initiative program No. 2010-0000712 of NRFK. Thanks to Mark Swinbank for the SMMJ2135-0102 SED. Thanks also to the anonymous referee for many helpful comments.

REFERENCES

Alexander D.M. et al. 2005, *Nature*, 434, 740
 Barger A.J. et al. 1998, *Nature*, 394, 248
 Bower R.G. et al. 2006, *MNRAS*, 370, 645
 Boyle B.J. & Terlevich R.J. 1998, *MNRAS*, 293, L49
 Calzetti D. et al. 2000, *ApJ*, 533, 682
 Chapman S.C. et al. 2005, *ApJ*, 622, 772
 Croton D.J. et al. 2006, *MNRAS*, 365, 11
 De Breuck C. et al. 2001, *AJ*, 121, 1241
 di Matteo T. et al. 2005, *Nature*, 433, 604

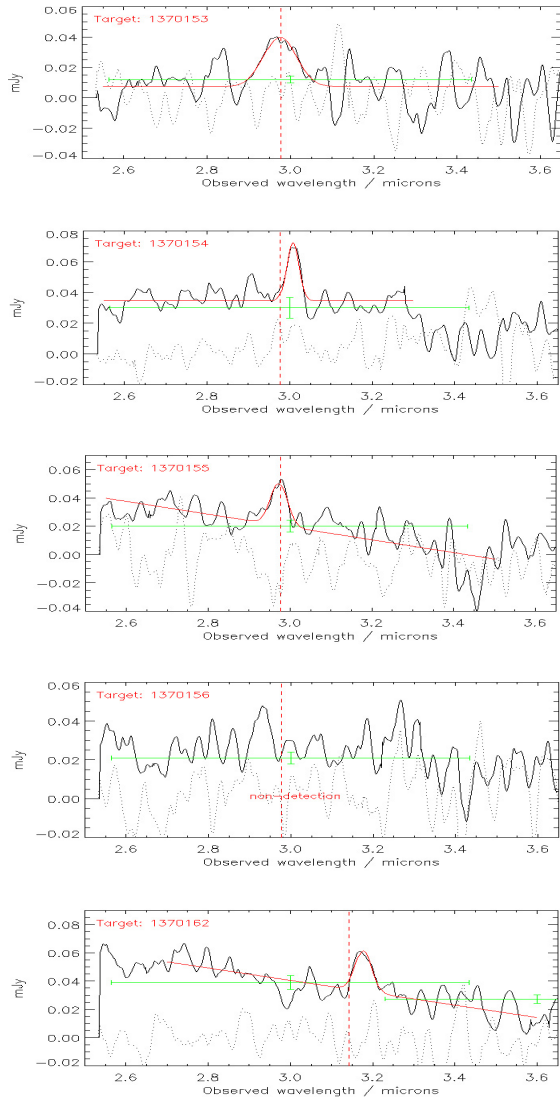


Figure 4. From top: 8C1909+722 HzRG, SMM1, SMM2, SMM3 (non-detection) and 4C60.07. The dashed red vertical lines show the position of $H\alpha$ emission lines at the expected redshifts. The solid red lines show the gaussian least-squares fits to the $H\alpha$ line and continuum in the wavelength region shown. The dotted grey lines show the noise levels as a function of wavelength, calculated as described in the text. The green points at $3.0 \mu\text{m}$ are from the *AKARI* broadband photometry (the reference image). The green point at $3.6 \mu\text{m}$ for 4C60.07 is from *Spitzer* IRAC broadband photometry. *Spitzer* photometry for 8C1909+722 is an order of magnitude higher and may include flux from another source; $0.8 \mu\text{m}$ Keck photometry (De Breuck et al. 2001) is the same order of magnitude as the *AKARI* data.

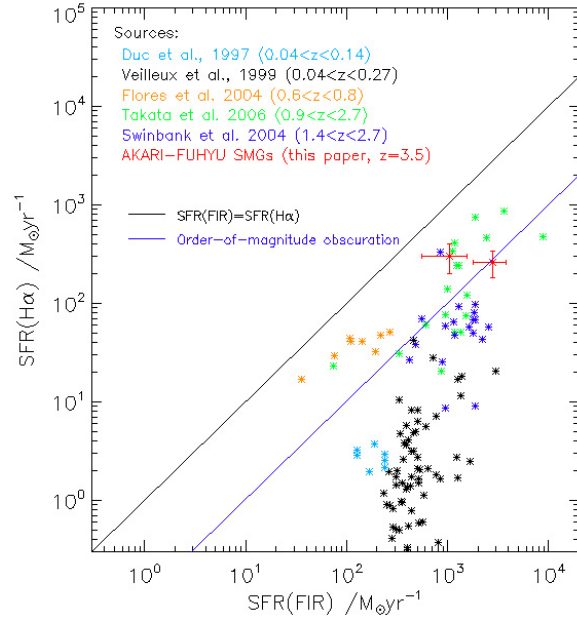
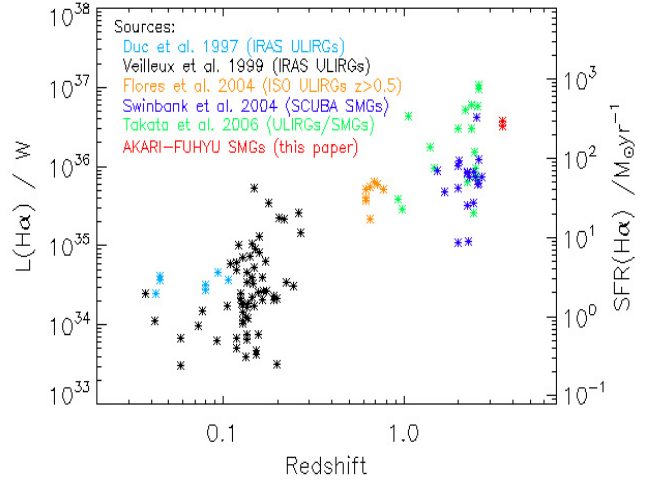


Figure 5. Top: $H\alpha$ luminosity for the two SMGs as a function of redshift in comparison with earlier studies. Bottom: Star formation rates based on $H\alpha$ luminosity versus far-infrared luminosity of the two SMGs compared that to those of recent studies. Takata et al. (2006) and Flores et al. (2004) data are shown before correction for extinction. Some sources show evidence of AGNs; all are SMGs. Our results are shown in red.

Djorgovski S. 1991, ASPC, 21, 349
 Duc P.A., Mirabel I.F. & Maza J. 1997, A&AS, 124, 533
 Ferrarese L., & Merritt D. 2000, ApJ, 539, L9
 Flores H., Hammer F., Elbaz D. et al. 2004, A&A, 415, 885
 Franceschini A. et al. MNRAS, 310, L5
 Gebhardt K. et al. 2000, ApJ, 539, L13
 Genzel R., Lutz D., Sturm E. et al. 1998, ApJ, 498, 579
 Greve T.R. et al. 2004, A&A, 419, 99
 Greve T.R., Ivison R.J. & Stevens J.A. 2006, AN, 327, 208

Harrison, C.M. et al. 2012, arXiv, 1209, 3016
 Hennawi J.F. et al. 2010, ApJ, 719, 1672
 Hughes D.H., Serjeant S., et al. 1998, Nature, 394, 241
 Ivison R.J. et al. 2008, MNRAS, 390, 1117
 Ivison R.J. et al. 2012, MNRAS accepted, arXiv, 1206, 4046
 Kayo I. & Oguri M. 2012, arXiv, 1203, 6410
 Kennicutt R.C. Jr. 1998, ARA&A, 36, 189
 Larkin J.E. et al. 2000, ApJ, 533, L61
 Magorrian J. et al. 1998, AJ, 115, 2285
 Murakami H. et al. 2007, PASJ, 59S, 369
 Nesvadba N.P.H. et al. 2011, A&A, 525, A43
 Onaka T. et al. 2007, PASJ, 59S, 401

- Onaka T. et al. 2009, AKARI IRC Data User Manual
Papadopoulos P.P. et al. 2000, ApJ, 528, 626
Pearson C.P., Serjeant S., Negrello M., et al. 2010, A&A, 514A, 9
Rawlings S. et al. 1995, MNRAS, 274, 428
Roettgering H.J.A. et al. 1997, A&A, 326, 505
Serjeant S. et al. 2008, MNRAS, 386, 1907
Smail I., Ivison R.J. & Blain A.W. 1997, ApJ, 490L, 5
Spoon H.W.W. et al. 2007, ApJ, 654, L49
Springel V. et al. 2005, MNRAS, 361, 776
Stevens J.A. et al. 2003, Nature, 425, 264
Swinbank A.M. et al. 2004, ApJ, 617, 64
Takata T. et al. 2006, ApJ, 651, 713
Veilleux S., Kim D.C., & Sanders D.B. 1999, ApJ, 522, 113